DOI: http://dx.doi.org/10.32571/ijct.755761 E-ISSN: 2602-277X

International Journal of Chemistry and Technology

http://dergipark.org.tr/ijct

Research Article

Silica-coated magnetic Fe_3O_4 nanoparticles as efficient nano-adsorbents for the improvement of the vapor-phase adsorption of benzene

Mehmet Şakir ECE [1,*], Sinan KUTLUAY[2], Ömer ŞAHİN[2]

[1]*Vocational High School of Health Services, Mardin Artuklu University, Mardin,47100, Turkey*

[2]*Department of Chemical Engineering, Faculty of Engineering, Siirt University, Siirt, 56100, Turkey*

Received: 21 June 2020; Revised: 13 April 2021; Accepted: 16 March 2021

*Corresponding author e-mail: sakirece@artuklu.edu.tr

Citation: Ece, M. Ş.; Kutluay, S.; Şahin, Ö. *Int. J. Chem. Technol.* **2021**, 5 (1), 33-41.

ABSTRACT

This study focused on the preparation of silica-coated Fe_3O_4 (Fe_3O_4@SiO_2) for the improvement of the vapor-phase adsorption of benzene. The Fe_3O_4@SiO_2 was prepared via the co-precipitation method, while its characterization was carried out using FT-IR, SEM and BET surface area analyses. The experimental parameters were evaluated for the vapor-phase adsorption of benzene using response surface methodology (RSM). The Fe_3O_4@SiO_2 adsorbed 197.50 mg g^{-1} of the vapor-phase benzene under the following optimum conditions: 39.93 min residence time, 13.57 mg l^{-1} initial benzene concentration and 26.87°C temperature. The vapor-phase adsorption mechanism of benzene on the Fe_3O_4@SiO_2 was clarified by investigating the isotherms including Dubinin-Radushkevich (D-R), Freundlich and Langmuir, and the experimenatal data were well fitted to the D-R model. The vapor-phase adsorption kinetics of benzene on the Fe_3O_4@SiO_2 was clarified by investigating the kinetics such as pseudo first-order (PFO) model and pseudo second-order (PSO) model, and the experimantal results obeyed the PSO model. This study demonstrated the application potential of magnetic Fe_3O_4@SiO_2 as promising low-cost nano-adsorbent.

Keywords: Fe_3O_4@SiO_2 magnetic nanoparticles, response surface methodology, vapor-phase adsorption of benzene.

Benzenin buhar-fazı adsorpsiyonunun iyileştirilmesi için etkili nano-adsorbentler olarak silika-kaplı manyetik Fe_3O_4 nanoparçacıkları

ÖZ

Bu çalışma, benzenin buhar-fazı adsorpsiyonunun iyileştirilmesi için silika-kaplı Fe_3O_4 (Fe_3O_4@SiO_2) hazırlanmasına odaklandı. Fe_3O_4@SiO_2 birlikte çökeltme yöntemi ile hazırlanırken karakterizasyonu FT-IR, SEM ve BET yüzey alanı analizleri kullanılarak gerçekleştirildi. Deneysel parametreler, yanıt yüzey metodolojisi (RSM) kullanılarak benzenin buhar-fazı adsorpsiyonu için değerlendirildi. Fe_3O_4@SiO_2, aşağıdaki optimum koşullar altında 197,50 mg g^{-1} buhar-fazı benzeni adsorbe etti: 39,93 dakika kalma süresi, 13,57 mg l^{-1} başlangıç benzen konsantrasyonu ve 26,87°C sıcaklık. Benzenin Fe_3O_4@SiO_2 üzerindeki buhar fazı adsorpsiyon mekanizması, Dubinin-Radushkevich (D-R), Freundlich ve Langmuir dahil izotermler incelenerek netleştirildi ve deneysel veriler D-R modeline iyi bir şekilde uyduruldu. Benzenin Fe_3O_4@SiO_2 üzerindeki buhar-fazı adsorpsiyon kinetiği, sözde birinci-dereceden (SBD) model ve sözde ikinci dereceden (SİD) model gibi kinetikler incelenerek netleştirildi, ve deneysel sonuçlar SİD modele uydu. Bu çalışma, Fe_3O_4@SiO_2'nin umut verici düşük maliyetli nano-adsorbent olarak uygulama potansiyelini gösterdi.

Anahtar Kelimeler: Benzenin buhar-fazı adsorpsiyonu, Fe_3O_4@SiO_2 manyetik nanoparçacıklar, yanıt yüzey metodu.

1. INTRODUCTION

Benzene, one of the important volatile organic compounds (VOCs), is an important material in chemical processing industries. VOCs are important air pollutants because of such detrimental effects as allergic reactions, nausea, throat irritation, nose, eye and headache. Besides, they cause dangerous environmental problems such as photochemical smog, suspended particulate matter, stratospheric ozone depletion and global warming.

DOI: http://dx.doi.org/10.32571/ijct.755761 E-ISSN: 2602-277X

Hence, VOCs with low concentrations have an important potential for environmental problem. This toxic product (benzene), which is extremely hazardous for human health and the environment, is emitted from automotive exhaust or fuels that evaporate from tanks, vehicle carburetors, and gas stations, particularly during oil refining operations, petrochemical production, and oil storage processes.[1-4] In general, the quality and amount of air pollutant emissions from the exhaust pipes are closely related to the fuel composition. Emissions from consumer products, building materials, paints, and adhesives are also influential in this situation. Besides, tobacco smoke is a source of this pollutant.[5] Industrial sectors considerably disrupt the gas rates in the air. The adverse effects on air quality create unfavorable conditions in terms of health. It is a necessity to decrease the entry of poisonous gases into the environmental atmosphere and to develop reduction strategies. To this end, pollutant removal methods have become essential. In this regard, nanotechnology presents effective solutions compared to traditional ones in adsorption technology as in all other fields.[6-7] In adsorption technology, magnetic nanomaterials with unique properties such as paramagnetism or ferromagnetism have drawn much attention. Magnetite (Fe_3O_4) is a common material widely examined in nanotechnological research.[8] It attracted considerable attention because of its magnetic properties such as biocompatibility, low-toxicity, low cost and high surface area.[9] Functionalization of Fe_3O_4 nanoparticles with functional groups both reduces agglomeration and provides new active sites for adsorption.[10-11] Fe_3O_4, which is one of many magnetic materials, facilitates recovery in the separation steps due to its magnetic feature. The pore volume of Fe_3O_4 nanoparticles has a well-developed pore structure producing a large number of active sites. Pore volume declines in the active areas due to agglomeration. Coating with organic or inorganic surfactants is a method to prevent particle agglomeration.[12] Silica (SiO_2) has extraordinary physical and chemical properties as an inorganic surfactant.[10]

This study focused on the preparation of silica-coated Fe_3O_4 (Fe_3O_4@SiO_2) magnetic nanoparticles and their application for the improvement of the vapor-phase adsorption of benzene. The Fe_3O_4@SiO_2 was prepared via the co-precipitation method, while its characterization was carried out using FT-IR, SEM and BET surface area analyses. Experimental parameters were evaluated for the vapor-phase adsorption of benzene by using the Box-Behnken design (BBD) with the response surface method (RSM). The vapor-phase adsorption mechanism of benzene on the Fe_3O_4@SiO_2 was clarified by investigating the isotherms including Dubinin-Radushkevich (D-R), Freundlich and Langmuir. The vapor-phase adsorption kinetics of benzene on the Fe_3O_4@SiO_2 was clarified by investigating the kinetics such as pseudo first-order (PFO) model and pseudo second-order (PSO) model.

2. MATERIALS AND METHODS

2.1. Materials

The tetraethyl orthosilicate (TEOS, $Si(OC_2H_5)_4$), benzene (C_6H_6), iron (II) chloride tetrahydrate ($FeCl_2.4H_20$), ethanol (CH_3CH_2OH), iron (III) chloride hexahydrate ($FeCl_3.6H_2O$), and ammonia (NH_3) were purchased from MERCK, ALFA AESAR, SIGMA-ALDRICH, MERCK, SIGMA-ALDRICH and VWR Chemical Companies, respectively. All solvents and chemicals employed in the study have analytical purity.

2.2. Preparation of the Fe_3O_4@SiO_2 magnetic nanoparticles

Fe_3O_4 was prepared by co-precipitation of Fe (III) and Fe (II). The mixture of $FeCl_2.4H_2O$ and $FeCl_3.6H_2O$ salts, in which the ratio of Fe^{+2}/Fe^{+3} was stoichiometrically 1/2, was mixed for 30 min at 80°C under argon gas in 50 ml deionized water. The color of the homogenized solution immediately became orange. 10 ml NH_3 solution was added drop-by-drop to obtain the co-precipitation. The color of the bulk solution instantly changed from orange to black. Amalgamation was continued under argon for 30 min. The Fe_3O_4 obtained as a product was washed five times with ethanol and deionized water. Fe_3O_4 was dried in a vacuum oven at 60°C for 24 h. 0.5 g of Fe_3O_4 was dispersed in a flask in 20 ml of deionized water, 5 ml of ammonia and 100 ml of ethanol. The solution of mixture was homogenized by ultrasonication for 30 min to create an uniform distribution. Then 0.4 ml of TEOS was added drop-by-drop to the solution under a strong mixture. The amalgamation was continued under argon gas for 12 h at room temperature. The Fe_3O_4@SiO_2, obtained as a product, was separated by a magnet, washed five times with deionized water and ethanol. The Fe_3O_4@SiO_2 was dried in a vacuum oven at 60°C for 24 h.[13] Schematic representation of the preparation of the Fe_3O_4@SiO_2 was presented in Figure 1.

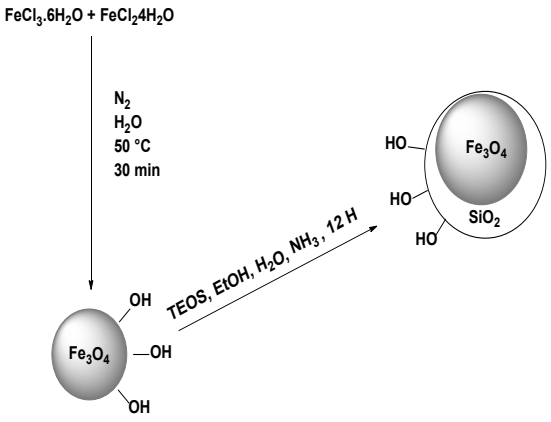

DOI: http://dx.doi.org/10.32571/ijct.755761 E-ISSN: 2602-277X

Figure 1. Schematic representation of the preparation of the Fe_3O_4@SiO_2 magnetic nanoparticles

2.3. Removal of benzene vapor by adsorption process

The adsorption process practiced in the removal of benzene vapor by using Fe_3O_4@SiO_2 magnetic nanoparticles was defined with the previously published study.[14] The nitrogen (N_2) flow rate for the removal of benzene vapor was chosen as 100 ml min^{-1}. The optimum dosage of Fe_3O_4@SiO_2 employed for the removal of benzene vapor was 0.09 g. The adsorption capacity, q (mg g^{-1}) for benzene vapor was defined with Eq. (1):[15]

$$q = \frac{F}{m}\int_0^t (C_{in} - C_{eff})dt \quad (1)$$

Here m is the optimum dosage of Fe_3O_4@SiO_2 (g), F is the flow rate (l min^{-1}), C_{in} and C_{eff} are the initial and output benzene vapor concentrations (mg l^{-1}), respectively, and t is the residence time (min).

2.4. Characterization

Fourier Transform Infrared Spectroscopy (FT-IR) spectra were taken using a Bruker-Vertex 70v FT-IR spectrometer. Scanning Electron Microscopy (SEM) images were taken by a ZEISS-EVO 50 instrument. Brunauer–Emmett–Teller (BET) surface area was determined by means of a Quantachrome-Nova instrument. Mathematical modeling for experimental data were conducted by applying Design Expert 12.0.8.0 Software (Free Trial Version).

3. RESULTS AND DISCUSSION

3.1. Characterization of the Fe_3O_4@SiO_2 magnetic nanoparticles

Characterization of the Fe_3O_4@SiO_2 magnetic nanoparticles was conducted based on SEM, FTIR, and BET surface area. SEM images, FTIR spectra and N_2 gas adsorption/desorption isotherms of these nanoparticles were presented in Figure 2, Figure 3, and Figure 4, respectively.

3.1.1. SEM analysis

SEM analysis was used to observe the surface morphology of the Fe_3O_4 and Fe_3O_4@SiO_2 magnetic nanoparticles. Figure 2 presented SEM microphotographs (scale length = 500 nm) of Fe_3O_4 and Fe_3O_4@SiO_2. It was understood that Fe_3O_4, which had good dispersion, had a rough surface. It was observed that the pore structure was rough and spongy. Pores and voids were clearly noticeable on the surface of Fe_3O_4@SiO_2. It was understood that the intrusions, protrusions, and roughness increased the surface area in the microstructure of the Fe_3O_4@SiO_2. Considering the scale length, it is understood that the diameters of the magnetic nanoparticle spheres are approximately 70-110 nm.[16]

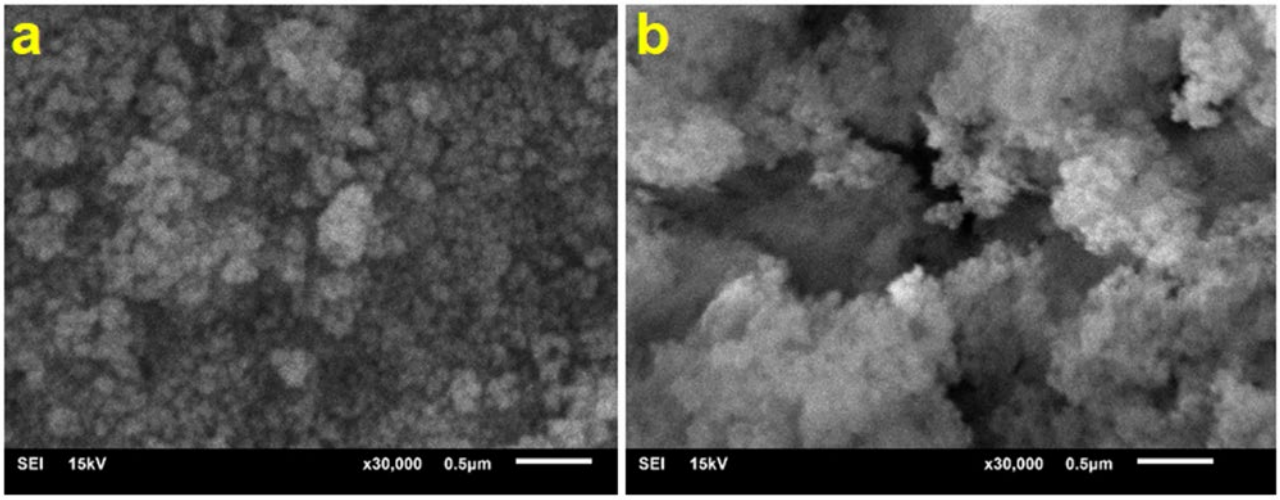

Figure 2. SEM images of the Fe_3O_4 (a) and Fe_3O_4@SiO_2 (b) magnetic nanoparticles.

3.1.2. FTIR analysis

FTIR spectra of Fe_3O_4 and Fe_3O_4@SiO_2 magnetic nanoparticles were presented in Figure 3. The characteristic absorption peak at 552 cm^{-1} observed in the FTIR spectrum of Fe_3O_4 belonged to the Fe-O bond, which verified the presence of Fe_3O_4. The peaks observed around 3446 cm^{-1}, 1654 cm^{-1} and 1480 cm^{-1} were peaks of stretching, bending, and deforming vibrations of the adsorbed water (-OH). The new peaks at 570 cm^{-1} and 964 cm^{-1} observed in the FTIR spectrum of the Fe_3O_4@SiO_2 were the peaks of the bending vibration of the Si-O bond and the stretching vibration of the Si-OH bond, respectively. The peak at 1082 cm^{-1} belonged to the asymmetric stretching vibration of the Si-O-Si bond. This peak indicated that the surface of Fe_3O_4 was successfully coated with SiO_2. The FTIR spectra observed for Fe_3O_4 and Fe_3O_4@SiO_2 complied with the literature.[17]

DOI: http://dx.doi.org/10.32571/ijct.755761 E-ISSN: 2602-277X

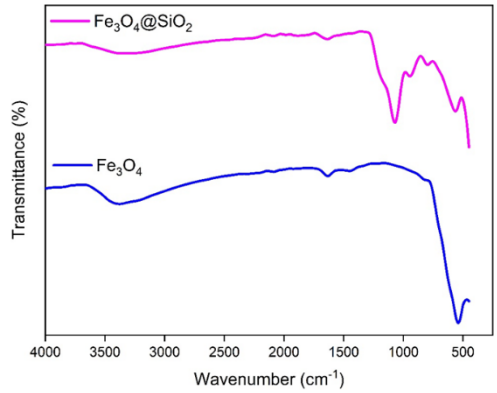

Figure 3. FT-IR spectrum of the Fe_3O_4 and Fe_3O_4@SiO_2 magnetic nanoparticles

3.1.3. BET analysis

The adsorption and desorption isotherms of Fe_3O_4@SiO_2 magnetic nanoparticles with BET surface area of 28.97 m^2 g^{-1} were presented in Figure 4. When Figure 4 was analyzed, it was understood that Fe_3O_4@SiO_2 fitted the H3 type hysteresis cycle and IV type curve according to the IUPAC classification criteria. It was also estimated that there were homogeneous mesoporous layers. The low surface area of Fe_3O_4@SiO_2 indicated that the surface area was affected by the SiO_2 modification. It was because SiO_2 was a shell of magnetic nanoparticles, and SiO_2 infiltrated into the spaces on the surface.

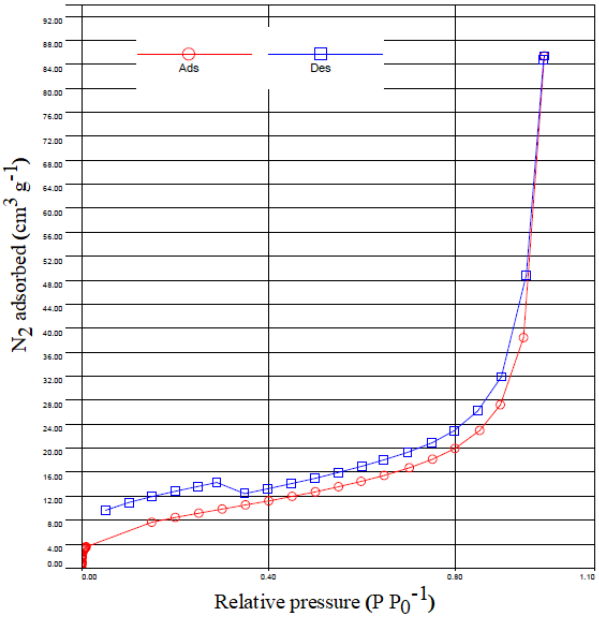

Figure 4. N_2 adsorption and desorption isotherms of the Fe_3O_4@SiO_2 magnetic nanoparticles

3.2. Experimental design and optimization

In the present study, RSM, which is an experimental method for the development, improvement, and optimization of the design process, was applied to determine the importance of the potential interactions of the functioning parameters. The approach of RSM-based BBD was employed to perform statistical analyses and obtain the regression model. In the vapor-phase adsorption of benzene, all statistical analyzes for modeling and optimization of experimental studies were evaluated. Effective parameters and interactions were evaluated by the program through variance analysis (ANOVA) and three-dimensional graphics. The general quadratic model equation was obtained with ANOVA test and BBD approach to analyze the relationship between the obtained results and parameters. The predicted adsorption capacity values were defined depending on the parameter values selected by employing the obtained quadratic model equation. The significance of the model predicted by the program was evaluated with the R^2 obtained, and the p-value, adeq precision and F-value results achieved by the program were analyzed. In the study, a three-variable BBD was used to determine the effect of different parameters upon response. The residence time, initial benzene concentration, and temperature were chosen as the essential independent parameters affecting the vapor-phase adsorption. The adsorption capacity of the vapor-phase benzene was considered as the response. The parameters analyzed in the BBD were displayed in three coded values. Experimental design levels with independent factors and the results obtained by the BBD approach were presented in Table 1 and Table 2 respectively. The compatibility of the results was presented with ANOVA analysis in Table 3. According to ANOVA results, the p-value of the proposed model was calculated as 0.0001, which shows that 99.99% of the results obtained in the laboratory conditions of the experiments predicted by the program can be defined with the model obtained with the program. Besides, the high R^2 value, F-value (>4), and adeq precision (>4) results, which were determined as 99.89, 678.81 and 80.50% respectively, showed that the experimental data well defined with the predicted model.[18-19] Besides, the fact that the actual and predicted adsorption capacities presented in Table 2 were close to each other indicated the suitability of the predicted model.

Table 1. Experimental design levels with independent factors

Factors	Coded values		
	-1	0	+1
Residencetime (X_1) (min)	20	30	40
Concentration (X_2) (mg l^{-1})	10	12.5	15
Temperature (X_3) (°C)	25	30	35

Figure 5 presented three-dimensional (3D) plots achieved with the program, showing the influence of initial benzene concentration, adsorption temperature and residence time on the vapor-phase adsorption capacity of benzene. It could be observed in Figure 5a that the vapor-phase adsorption capacity of benzene increased with the increase in residence time.

DOI: http://dx.doi.org/10.32571/ijct.755761 E-ISSN: 2602-277X

Table 2. Experiment design results obtained for the vapor-phase adsorption of benzene by the $Fe_3O_4@SiO_2$ magnetic nanoparticles.

Run	Time (min)	Concentration (mg l^{-1})	Temperature (°C)	Actual adsorption capacity (mg g^{-1})	Predicted adsorption capacity (mg g^{-1})
1	30	12.5	30	80	83
2	20	15	30	50	57
3	20	10	30	41	40
4	30	15	35	60	58
5	40	12.5	35	150	162
6	30	12.5	30	80	86
7	20	12.5	25	45	53
8	40	15	30	185	190
9	40	10	30	160	157
10	30	12.5	30	82	85
11	30	15	25	110	116
12	40	12.5	25	198	201
13	30	10	25	70	68
14	30	12.5	30	80	89
15	30	10	35	55	57
16	20	12.5	35	36	28
17	30	12.5	30	80	85

Table 3. ANOVA results created in accordance with the BBD approach

Source	Sum of squares	df	F-value	p-value	
Model (quadratic)	20627.11	9	678.81	< 0.0001	Significant
X_1	8532.50	1	5005.50	< 0.0001	
X_2	8247.96	1	115.09	< 0.0001	
X_3	191.84	1	274.47	< 0.0001	
X_1X_2	1545.57	1	9.44	0.0180	
X_1X_3	0.0071	1	56.10	0.0001	
X_2X_3	3.64	1	45.18	0.0003	
X_1^2	1242.51	1	598.85	< 0.0001	
X_2^2	1181.88	1	3.73	0.0948	
X_3^2	472.13	1	10.96	0.0129	

$R^2 = 0.9989$, Adeq precision = 80.50

The adsorption process reached equilibrium after a specific residence time because of the limited number of active areas on the surface of $Fe_3O_4@SiO_2$.[20] As observed in Figure 5b, the temperature had an adverse effect on vapor-phase adsorption. Adsorption capacity decreased as the temperature rose. Also, it could be said that the decrease in the amount adsorbed with the increased temperature might be caused by the destruction of the active bond sites on the adsorbent.[21] When the surface plot for the initial benzene concentration versus temperature in Figure 5c was considered, it was evident that the initial benzene concentration did not have a meaningful effect on the vapor-phase adsorption capacity. The increase seen in the vapor-phase adsorption of benzene was caused by the less interest in $Fe_3O_4@SiO_2$. Similar behaviors have been observed in previous studies.[14, 22]

Process parameters were optimized to define the vapor-phase adsorption capacity of benzene by applying $Fe_3O_4@SiO_2$. Based on the model equation for the actual values predicted by the quadratic model, the mathematically optimum conditions were defined. With the help of the predicted model equation, optimum values were determined to be 39.93 min for residence time, 13.57 mg l^{-1} for initial benzene concentration, and 26.87°C for temperature. The vapor-phase adsorption capacity of benzene with $Fe_3O_4@SiO_2$ was determined as 197.50 mg g^{-1}.

DOI: http://dx.doi.org/10.32571/ijct.755761 E-ISSN: 2602-277X

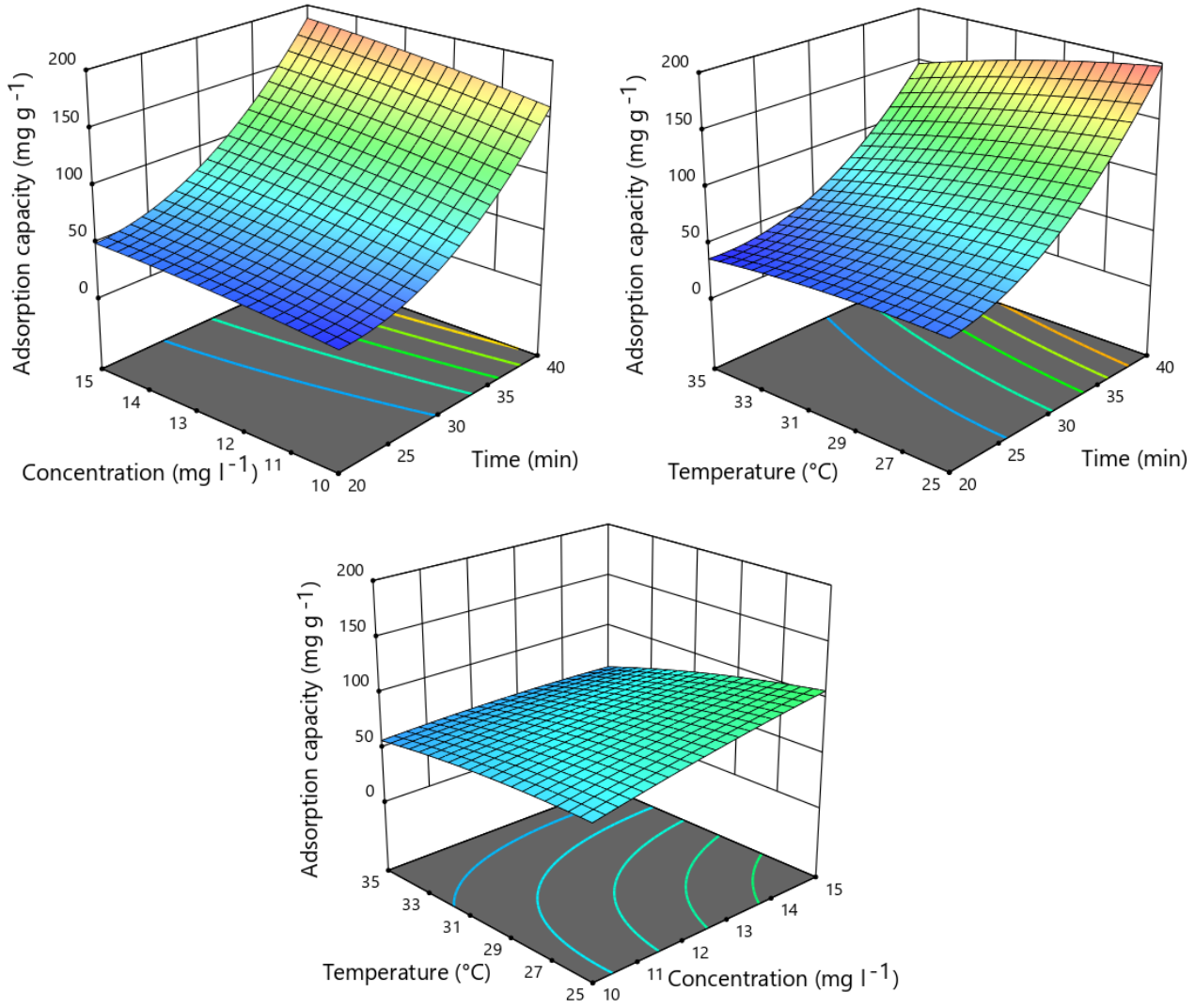

Figure 5. The influence of parameters on the vapor-phase adsorption capacity of benzene.

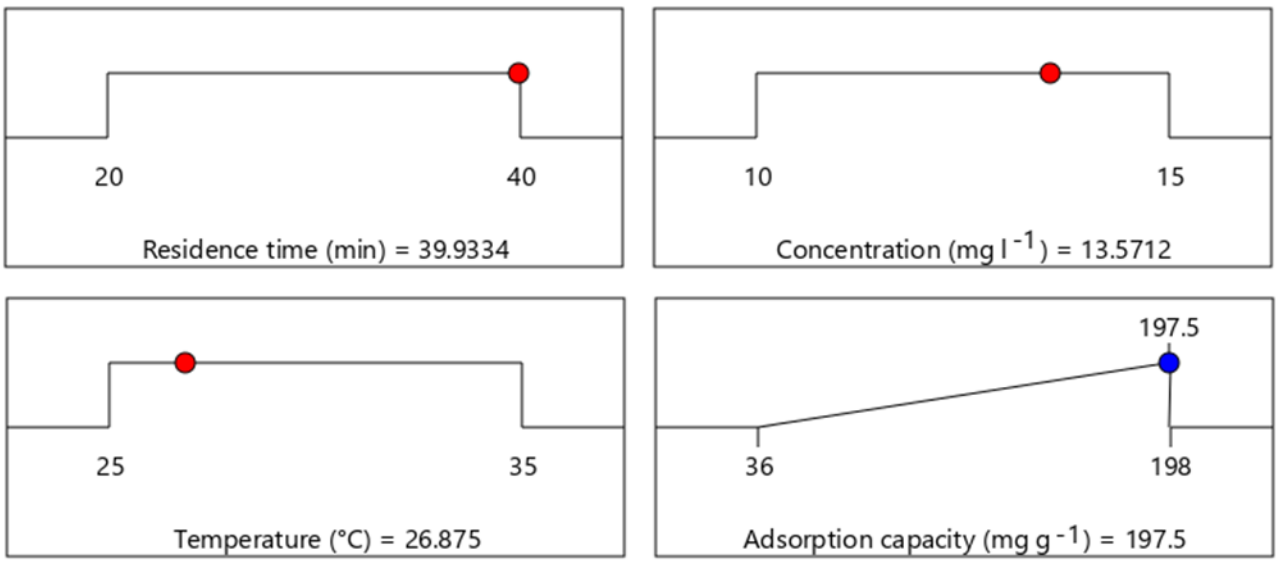

Figure 6. Optimum values for the vapor-phase adsorption of benzene

DOI: http://dx.doi.org/10.32571/ijct.755761 E-ISSN: 2602-277X

3.3. Kinetic studies

Under optimum conditions defined by RSM, the vapor-phase adsorption kinetics of benzene on the Fe_3O_4@SiO_2 was clarified by investigating the kinetics such as pseudo first-order (PFO) model and pseudo second-order (PSO) model. PFO model defines the adsorption rate proportional to the number of empty sites.[23] PFO model was related to the change of concentration over time. The non-linear form of the PFO model kinetic equation was presented in Eq. (2). The PSO model equation, based on the capacity of the adsorption equilibrium, suggests that the rate of adsorption is related to the concentration of active sites on the surface of the adsorbent.[23] The non-linear form of the PSO model was given with the Eq. (3).[24]

$$q_t = q_e(1 - e^{-k_f t}) \quad (2)$$

$$q_t = \frac{k_s q_e^2 t}{1 + k_s q_e t} \quad (3)$$

Where, q_e and q_t indicate the adsorption capacity at equilibrium and t time (mg g^{-1}), respectively, and k_f represents the PFO model rate constant (1 min^{-1}), k_s is the PSO model rate constant (g mg^{-1} min^{-1}).

In the vapor-phase adsorption process of benzene by the Fe_3O_4@SiO_2, the experimantal results obeyed the PSO model (Figure 7 and Table 4).

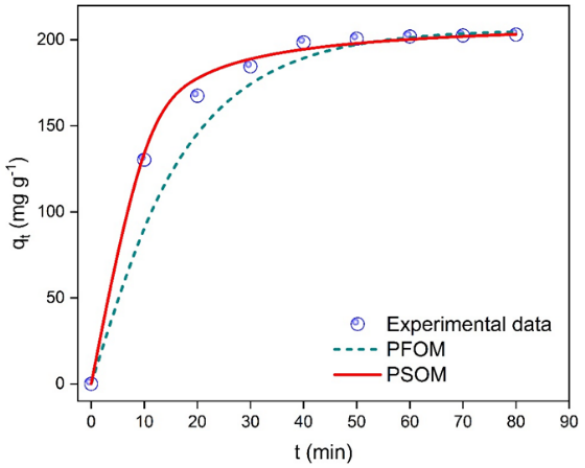

Figure 7. Adsorption kinetic models of benzene by the Fe_3O_4@SiO_2 magnetic nanoparticles

Table 4. Adsorption kinetic parameters of benzene by the Fe_3O_4@SiO_2 magnetic nanoparticles

Kinetic models	Parameters	Values
PFO model	q_e	205.952
	k_f	0.0648
	R^2	0.967
PSO model	q_e	212.45
	k_s	0.0013
	R^2	0.990

3.4. Isotherm studies

Under optimum conditions defined by RSM, The vapor-phase adsorption mechanism of benzene on the Fe_3O_4@SiO_2 was clarified by investigating the isotherms including Dubinin-Radushkevich (D-R), Freundlich and Langmuir. The Langmuir adsorption isotherm applies to single-layer surface adsorption, including a limited number of identical regions. The model assumes that the adsorption energies on the surface are the same and that there is no adsorbate migration at the surface plane. Based on these assumptions, the Langmuir model is formulated in Eq. (4). The Freundlich isotherm theory puts forward that the ratio of the amount of solute adsorbed on a particular sorbent mass to the concentration of the solute is not constant at different concentrations. The non-linear form of the Freundlich isotherm model was given in Eq. (5).[25] The D-R isotherm model was developed to describe the effect of the porous structure of adsorbents. It is based on the theory of the adsorption potential and suggests that in contrast to the layered adsorption on pore walls, the adsorption process is associated with the filling of the microporous volume.[26-27] The non-linear form of this model was presented in Eq. (6).[28] In Eq. (6), β gives E which represents the average free energy of adsorption per particle. E was presented in Eq. (8).[28]

$$q_e = \frac{q_{max}\ K_L\ C_e}{1 + K_L\ C_e} \quad (4)$$

$$q_e = K_F C_e^{\frac{1}{n}} \quad (5)$$

$$q_e = q_m\ exp(-\beta\varepsilon^2) \quad (6)$$

$$\varepsilon = RTln\left(1 + \frac{1}{C_e}\right) \quad (7)$$

$$E = \frac{1}{\sqrt{2\beta}} \quad (8)$$

Where, C_e (mg l^{-1}) is the equilibrium concentration of the adsorbate, q_e (mg g^{-1}) is the adsorption capacity at equilibrium, q_{max} (mg g^{-1}) is the maximum monolayer adsorption capacity, K_L (l mg^{-1}) is Langmuir isotherm constant, K_F [(mg g^{-1}) (l $mg^{-1})^{1/n}$] is the Freundlich isotherm constant, n is the adsorption density, if n is between 1 and 10, this situation indicates a suitable adsorption process, q_m is the maximum adsorption capacity (mg g^{-1}), β is the activity coefficient constant (mol^2 kJ^{-2}), ε is the polanyi potential (J mol^{-1}), R and T represent the gas constant (8.314 J mol^{-1} K^{-1}), absolute temperature (K), respectively, If E < 8 kJ mol^{-1}, physical adsorption is dominant. However, in the situation indicating 8 kJ mol^{-1} < E <16 kJ/mol and E >16 kJ mol^{-1}, adsorption occurs by ion exchange and diffusion, respectively.[29]

In the study, the estimated q_{max} from the Langmuir model was 237.192 mg g^{-1}, K_L was 0.281 l mg^{-1}. The R^2 value

DOI: http://dx.doi.org/10.32571/ijct.755761 E-ISSN: 2602-277X

was 0.999, indicating the equilibrium isotherm data of benzene in the vapor-phase adsorption process by the Fe_3O_4@SiO_2 better fitted to the D-R model. The calculated *E* value in the study was determined as 0.463 kJ mol^{-1}, indicating that the vapor-phase adsorption process of benzene was physical (Figure 8 and Table 5). In addition, the n value of Freundlich model was calculated as 3.472, indicating that the vapor-phase adsorption process of benzene was suitable.[30]

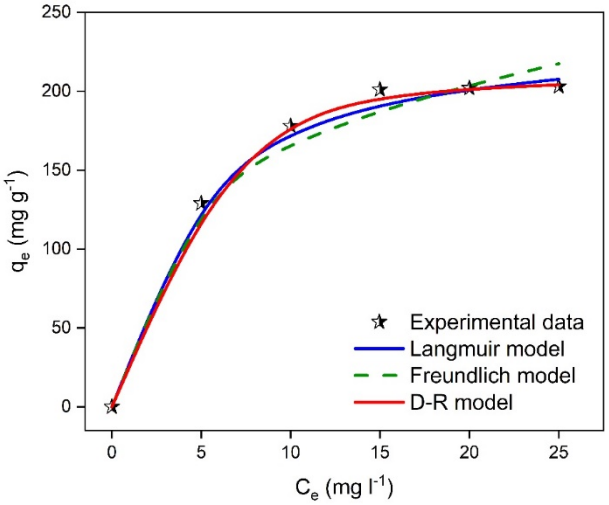

Figure 8. Adsorption isotherm models of benzene by the Fe_3O_4@SiO_2 magnetic nanoparticles

Table 5. Adsorption isotherm parameters of benzene by the Fe_3O_4@SiO_2 magnetic nanoparticles

Isotherm models	Parameters	Values
Langmuir	q_{max}	237.192
	K_L	0.281
	R^2	0.997
Fruendlich	K_F	86.056
	n	3.472
	R^2	0.991
D-R	q_m	208.721
	β	$2.334*10^{-6}$
	E	0.463
	R^2	0.999

4. CONCLUSIONS

The present study focused on the preparation of Fe_3O_4@SiO_2 for the improvement of the vapor-phase adsorption of benzene. The Fe_3O_4@SiO_2 was prepared via the co-precipitation method, while its characterization was carried out using FT-IR, SEM and BET surface area analyses. The experimental parameters were evaluated for the vapor-phase adsorption capacity of benzene using BBD under RSM. The Fe_3O_4@SiO_2 adsorbed 197.50 mg g^{-1} of the vapor-phase benzene under the following optimum conditions: 39.93 min residence time, 13.57 mg l^{-1} initial benzene concentration and 26.87°C temperature. The vapor-phase adsorption mechanism of benzene on the Fe_3O_4@SiO_2 was clarified by investigating the isotherm models such as Dubinin-Radushkevich (D-R), Freundlich and Langmuir, and the experimenatal data were well fitted to the D-R model. The vapor-phase adsorption kinetics of benzene on the Fe_3O_4@SiO_2 was clarified by investigating the kinetics such as PFO model and PSO model, and the experimantal results obeyed the PSO model. This study demonstrated the application potential of magnetic Fe_3O_4@SiO_2 as promising low-cost nano-adsorbents for the vapor-phase adsorption of benzene.

ACKNOWLEDGEMENTS

The authors are grateful to the Mardin Artuklu University Research Fund (MAUBAP, Project No. MAÜ.BAP.18.SHMYO.030) for their financial support.

Conflict of interests

I declare that there is no a conflict of interest with any person, institute, company, etc.

REFERENCES

1. Ece, M. Ş.; Kutluay, S.; Şahin, Ö.; Horoz, S. *Ind. Eng. Chem. Res.* **2020,** *59* (48), 21106-21123.

2. Kutluay, S. *Fuel* **2021,** *287*, 119691.

3. Kutluay, S.; Temel, F. *Colloid Surf. A-Physicochem. Eng. Asp.* **2021,** *609*, 125848.

4. Şahin, Ö.; Kutluay, S.; Horoz, S.; Ece, M. Ş. *Environ. Sci. Pollut. Res.* **2021,** *28* (5), 5231-5253.

5. Wallace, L. A. *Environ. Health Perspect.* **1989,** *82*, 165-169.

6. Yang, X.; Yi, H.; Tang, X.; Zhao, S.; Yang, Z.; Ma, Y.; Feng, T.; Cui, X. *J. Environ. Sci.* **2018,** *67*, 104-114.

7. Wibowo, N.; Setyadhi, L.; Wibowo, D.; Setiawan, J.; Ismadji, S. *J. Hazard. Mater.* **2007,** *146* (1-2), 237-242.

8. de las Nieves Piña, M.; Rodríguez, P.; Gutiérrez, M. S.; Quiñonero, D.; Morey, J.; Frontera, A. *Chem. Eur. J.* **2018,** *24* (49), 12820-12826.

9. Connie, Z. Y.; Ariya, P. A. *J. Environ. Sci.* **2015,** *31*, 164-174.

10. Roto, R.; Yusran, Y.; Kuncaka, A. *Appl. Surf. Sci.* **2016,** *377*, 30-36.

11. Mohamed, E. F. *Environ. Dev. Sustain.* **2017,** *6* (2).

12. Duan, S.; Xu, X.; Liu, X.; Wang, Y.; Hayat, T.; Alsaedi, A.; Meng, Y.; Li, J. *J. Colloid Interface Sci.* **2018,** *513*, 92-103.

13. Zandipak, R.; Sobhan Ardakani, S.; Shirzadi, A. *Sep. Sci. Technol.* **2020,** *55* (3), 456-470.

14. Kutluay, S.; Baytar, O.; Şahin, Ö. *J. Environ. Chem. Eng.* **2019,** *7* (2), 102947.

15. Zhao, Z.; Wang, S.; Yang, Y.; Li, X.; Li, J.; Li, Z. *Chem. Eng. J.* **2015,** *259*, 79-89.

DOI: http://dx.doi.org/10.32571/ijct.755761 **E-ISSN: 2602-277X**

16. Yousefi, V.; Tarhriz, V.; Eyvazi, S.; Dilmaghani, A. *J. Nanobiotechnology* **2020,** *18* (1), 155.

17. Ma, C.; Li, C.; He, N.; Wang, F.; Ma, N.; Zhang, L.; Lu, Z.; Ali, Z.; Xi, Z.; Li, X. *J. Biomed. Nanotechnol.* **2012,** *8* (6), 1000-1005.

18. Kutluay, S.; Ece, M. Ş.; Şahin, Ö. *Int. J. Chem. Technol.* **2020,** *4* (2), 146-155.

19. Temel, F.; Kutluay, S. *New J. Chem.* **2020,** *44* (30), 12949-12961.

20. Vohra, M. S. *Arab. J. Sci. Eng.* **2015,** *40* (11), 3007-3017.

21. Padmavathy, V. *Bioresour. Technol.* **2008,** *99* (8), 3100-3109.

22. Kutluay, S.; Baytar, O.; Şahin, Ö. *Res. Eng. Struct. Mater.* **2019,** *5* (3), 279-298.

23. Ali, R. M.; Hamad, H. A.; Hussein, M. M.; Malash, G. F. *Ecol. Eng.* **2016,** *91*, 317-332.

24. Vora, S.; Khimani, M.; De, C. *Ecol. Eng.* **2013,** *34* (7), 947-956.

25. Salih, W. M.; Gzar, H. A.; Hassan, N. F. *J. Eng.* **2012,** *18* (9), 1042-1054.

26. Laskar, I. I.; Hashisho, Z. *Sep. Purif. Technol.* **2020**, 116681.

27. Abbas, A.; Abussaud, B. A.; Al-Baghli, N. A.; Khraisheh, M.; Atieh, M. A. *J. Nanomater.* **2016,** *2016*.

28. Hu, Q.; Zhang, Z. *J. Mol. Liq.* **2019,** *277*, 646-648.

29. Sadeghalvad, B.; Azadmehr, A.; Hezarkhani, A. *RSC Adv.* **2016,** *6* (72), 67630-67642.

30. Wang, C.; Zhong, H.; Wu, W.; Pan, C.; Wei, X.; Zhou, G.; Yang, F. *ACS Omega* **2019,** *4* (1), 1652-1661.